

# The incidence of mid-infrared excesses in G and K giants

Mark H. Jones <sup>\*</sup>

*Department of Physics and Astronomy, The Open University, Walton Hall, Milton Keynes, MK7 6AA*

in original form 2008 February 6

## ABSTRACT

Using photometric data from the 2MASS and GLIMPSE catalogues, I investigate the incidence of mid-infrared excesses ( $\sim 10\ \mu\text{m}$ ) of G and K stars of luminosity class III. In order to obtain a large sample size, stars are selected using a near-IR colour-magnitude diagram. Sources which are candidates for showing mid-IR excess are carefully examined and modelled to determine whether they are likely to be G/K giants. It is found that mid-IR excesses are present at a level of  $(1.8 \pm 0.4) \times 10^{-3}$ . While the origin of these excesses remains uncertain, it is plausible that they arise from debris discs around these stars. I note that the measured incidence is consistent with a scenario in which dust lifetimes in debris discs are determined by Poynting-Robertson drag rather than by collisions.

**Key words:** infrared: stars – circumstellar matter.

## 1 INTRODUCTION

It has long been recognised (e.g. Jura 1999) that the presence of infrared excesses in giant stars which have yet to evolve up the asymptotic giant branch may be due to the presence of long-lived debris discs around these stars. Recent work on debris discs has concentrated on their properties during the main-sequence phase of stellar evolution but is becoming clear that some debris discs survive into the post-main sequence lives of stars, as exemplified by the white dwarfs G29-38 and GD 362 (Zuckerman & Becklin 1987; Becklin et al. 2005), and possibly around the central star of the Helix Nebula (Su et al. 2007). The presence of detectable discs around evolved stars may provide useful information about processes in debris discs since they have radiation environments which are distinct from systems in which the host star is on the main-sequence. The study of debris discs might be especially fruitful for giant stars which have yet to ascend the asymptotic giant branch, since infrared emission is unlikely to be contaminated by emission from dust which has been lost from the star itself.

To date, several studies have been made into the incidence of infrared excesses in giants. In the main, these studies have concentrated on the far-IR emission from giant stars. An important result from Plets & Vynckier (1999), which is based on detailed analysis of data from the *IRAS* Faint Source Catalog (Moshir et al. 1992), is that the incidence of  $60\ \mu\text{m}$  excesses in giants of spectral type G and K is  $14 \pm 5$  per cent.

In the mid-IR (i.e. wavelengths of order  $10\ \mu\text{m}$ ), the incidence of excesses in G/K giants is not well determined.

There have been indications that there are some such stars which do exhibit mid-IR excesses. For example, a study by Clarke, Oudmaijer & Lumsden (2005), identifies four stars with spectral type G or K and with luminosity class III which show an excess at wavelengths of  $8\ \mu\text{m}$ . Another example of a G/K giant which shows mid-IR excesses is HD 233517, which was subject to mid-IR spectroscopic observations using *Spitzer* by Jura et al. (2006), who concluded that this is likely to be a binary system with a peculiar history.

An indication that some G/K giants may have mid-IR excesses is also evident from a study of mid-IR extinction by Indebetouw et al. (2005). These authors noted, in passing, that in a selected sample of red-clump stars (which correspond to G/K giants) there appeared to be a small proportion of stars which exhibit excesses at  $8\ \mu\text{m}$  in comparison to measured  $K_S$  magnitudes (see their figure 4). Indebetouw et al. attributed these mid-IR excesses to circumstellar dust but did not examine this population in detail. In particular, little attention was paid by these authors as to whether the stars with mid-IR excess are actually G/K giants. In this work I investigate a similarly selected population of stars, but take considerable care in the selection of such a population and to pay particular attention to determining the nature of stars which show mid-IR excesses.

The aim of this study is to determine the incidence of excesses at  $8\ \mu\text{m}$  in G and K giants, and to use available near- and mid-infrared photometry to investigate the nature of the sources showing such excesses. The most straightforward approach to such a study would be to cross-correlate a large spectral class catalogue, such as the Tycho-2 Spectral Catalog (Wright et al. 2003) with a mid-IR catalogue such as the GLIMPSE Catalog (Benjamin et al. 2003). This

<sup>\*</sup> e-mail: m.h.jones@open.ac.uk

approach was investigated but was found to be limited by the fact that the number of spectroscopically identified G/K giants returned by such a cross-matching is only of order of a few hundred, and of these, many are relatively bright and hence are saturated in one or more photometric bands of the *Spitzer* IRAC instrument. So, while this approach is satisfactory for investigating mid-IR excesses in main-sequence stars (and is the approach adopted by Uzpen et al. 2007) it returns too few matches to provide any useful information on the incidence of such excesses in G/K giants.

The approach adopted here is to use a near-IR colour-magnitude diagram to select a large sample (about  $10^4$ ) of red-clump stars, and then to investigate in detail the stars from this sample which exhibit mid-IR excesses. In particular, I attempt to ascertain whether their spectral energy distributions are consistent with being G/K giants with excesses due to circumstellar dust and to rule out other plausible types of source.

This paper is structured as follows: Section 2 describes the data sets and the survey region adopted for this study and how a sample of red-clump giants was selected. Section 3 reports on the subset of these sources which are identified as having a mid-IR excess. The implications of the observed incidence of genuine mid-IR excesses in G/K giants is discussed in Section 4.

## 2 DATA SETS AND SURVEY REGION

The basis of this study is to use a near-infrared colour-magnitude (CM) diagram to select a population of objects which have a high probability of being G or K giants. A distinctive feature of any deep CM diagram of a sample which contains evolved stars of near-solar metallicity is the presence of a feature arising from the so-called red-clump, which corresponds to the core-helium burning phase of intermediate mass stars. Studies of the properties of red-clump giants, such as by Zhao, Qiu & Mao (2001) identify such stars as being of spectral type G or K and of luminosity class III (I shall use the terms red-clump stars and G/K giants interchangeably here). Stars which can be identified as belonging to this population have been used in a variety of contexts as standard candles; for instance, to study Galactic structure (López-Corredoira et al. 2002). In this study, the identification of red-clump stars is used as a basis for studying the properties of the stars themselves. In particular, the near-IR CM diagram is used to select a population of stars for which near and mid-IR photometry is available.

A common choice of photometric bands which can be used to construct the required CM diagram is the near-IR  $J$  and  $K$  bands. In this study I use data from the 2MASS Point Source Catalog (Skrutskie et al. 2006), which comprises  $J$ ,  $H$  and  $K_S$  photometric bands ( $K_S$  overlaps with the standard  $K$  band, but is slightly narrower and has a centre-of-band wavelength of  $2.15\ \mu\text{m}$ ). Figure 1 shows the  $(J - K_S)$  versus  $K_S$  colour magnitude diagram for the chosen survey region (a description of which is given below). In this diagram, the red-clump stars form the band of sources stretching from  $(J - K_S) \approx 1.0$ ,  $K_S \approx 11$ , down and to the right towards  $(J - K_S) \approx 1.8$ ,  $K_S \approx 14$ .

The identification of this feature with G/K giants is supported by its proximity to the expected locus of red-clump

stars given a reasonable model for extinction along lines of sight in the survey region. If it is assumed that the extinction per unit distance in the  $K_S$  band,  $c_K$ , is uniform, then for a given value of  $c_K$ , the tracks followed by different spectral classes of stars can be determined. Adopting the values given by López-Corredoira et al. (2002) for canonical red-clump giants, that the absolute  $K_S$  magnitude  $M_K = 1.65$  and the un-reddened colour  $(J - K_S)_0 = 0.75$ , it is found that a good match between the red-clump feature and the expected location of such stars is obtained for  $c_K \approx 0.09\ \text{mag kpc}^{-1}$  (indicated by the track labelled ‘RCG’ in Figure 1). This value of  $c_K$  is in good agreement with the extinction data of Marshall et al. (2006) for the chosen survey region when determined over scales of several kiloparsecs.

To the left and slightly below this feature (which I refer to as the red-clump band), the sources which have  $(J - K_S)$  in the range from 0 to about 1, are likely to be main sequence stars (Bessell & Brett 1988), with later type stars showing relatively less reddening due to their proximity to the Sun. To the right of the red-clump band the CM diagram is populated by giants ascending the giant branch and the asymptotic giant branch. The degree of discrimination between red-clump giants and later type giants is illustrated in Figure 1, which also shows the expected loci of stars of type M0III and M5III (with  $(J - K_S)$  colours as given by Bessell & Brett 1988, and absolute magnitudes derived from values given by Cox 2000) under the assumption of the same extinction model as adopted for the displayed locus of RCG stars. It can be concluded that the red-clump is a clearly defined feature in the colour-magnitude diagram.

The survey area for this study was selected such that mid-IR photometry could be obtained from the GLIMPSE Catalog (Benjamin et al. 2003)<sup>1</sup>. GLIMPSE is a survey of the Galactic plane ( $10^\circ \leq |l| \leq 65^\circ$  and  $|b| \leq 1.0^\circ$ ) made using the four wavelength bands (3.6, 4.5, 5.8 and  $8.0\ \mu\text{m}$ ) of the IRAC instrument on *Spitzer* (Fazio et al. 2004). A preliminary study for this work was based on the Version 1 release of the GLIMPSE catalogues (released April 2005), while the results presented here are based on the Version 2 release (April 2007) unless otherwise indicated.

Any direction in the GLIMPSE survey region has a long line-of-sight through the disc of the Galaxy. This is advantageous in terms of the numbers of red-clump stars that can be detected, but, of course, the survey regions are subject to relatively high levels of extinction. Such extinction, corresponding to column densities of order a few  $\times 10^{21}\ \text{H atoms cm}^{-2}$ , is not an issue as such, but it is important to appreciate that variation of extinction across a survey region will lead to a loss of definition (i.e. a broadening) of the red-clump band in the resulting CM diagram. In choosing any extended survey area, some variation of extinction is inevitable, but this variation can be reduced by excluding regions with a high content of molecular gas. In choosing the survey region, the aim was to maximise the area covered subject to the constraint of avoiding regions of high column density in molecular gas. This was done by avoiding known star formation regions, and by choosing a region of relatively low column density in

<sup>1</sup> All GLIMPSE data products were obtained from <http://www.astro.wisc.edu/sirtf/glimpsedata.html>

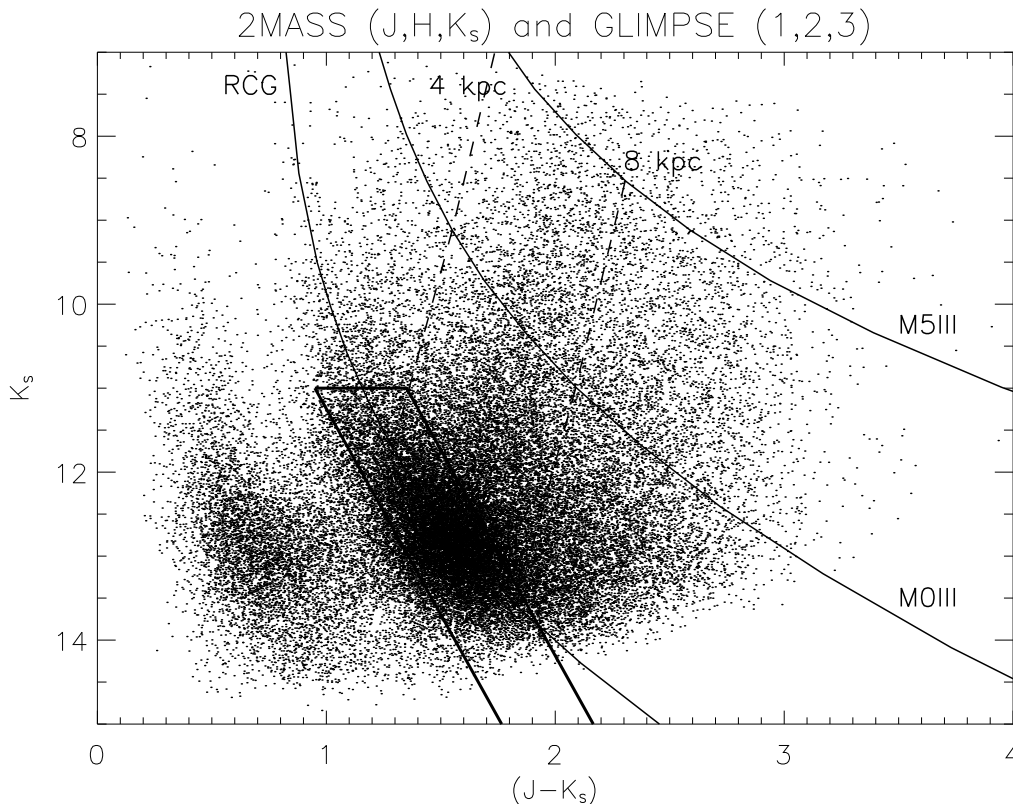


**Figure 1.** The  $K_S$  versus  $(J - K_S)$  colour-magnitude diagram of the survey area. Sources included in this diagram are those which have photometric data in 2MASS at  $J$ ,  $H$ , and  $K_S$  and GLIMPSE at 3.6, 4.5 and 5.8  $\mu\text{m}$ ). The solid curves indicate the loci expected for red-clump giants (RCG) and M giants under the assumption of uniform extinction per unit distance in the  $K_S$  band of  $0.09 \text{ mag kpc}^{-1}$ , with distances of 4 and 8 kpc indicated by dashed lines. The parallelogram (heavy lines) indicates the criteria used to select red-clump sources from this sample (see text for details).

molecular hydrogen from inspection of the CO emission map of Dame, Hartmann & Thaddeus (2001). The region used for this study is defined by  $45.0^\circ \leq (l) \leq 50.25^\circ$  and  $0.70^\circ \leq (b) \leq 1.0^\circ$ . For the area covered by the GLIMPSE survey, the selected region has relatively low column densities of CO.

The number of 2MASS sources with measured values of  $J$  and  $K_S$  in the selected region is 93888. The extent of the survey area is such that about  $10^4$  clump giants would be included in the final sample, which is sufficient to measure the incidence of mid-IR excesses at a level of order 0.1 per cent.

## 2.1 Selection of red-clump sources

As noted above, the selection of red-clump sources is based on the  $(J - K_S)$ - $K_S$  CM diagram. Rather than using all sources with 2MASS  $J$  and  $K_S$  data, preliminary studies revealed that an improvement in the degree of contrast between the red-clump and the main sequence features can be achieved by requiring that included sources are detected in all 2MASS bands and the 3.6, 4.5 and 5.8  $\mu\text{m}$  bands of the GLIMPSE Catalog. The number of sources in the survey region which satisfy this criterion is 53520 and it is these sources which are shown in the CM diagram in Figure 1.

Stars which have a high probability of being G/K giants were selected by following the leftmost side of the

red-clump band which is evident in Figure 1. While such a selection is somewhat subjective, using the left-hand side of the red-clump distribution in this way should minimise contamination of the sample from stars ascending the giant branch/asymptotic giant branch. The selection criterion used was that  $K_S \geq 11.0$  and that  $(J - K_S)$  should lie within  $\pm 0.2$  magnitudes of the straight line defined by

$$(J - K_S) = 1.15 + 0.204(K_S - 11.0) \quad (1)$$

This selection region is overlaid on Figure 1. Note that the cutoff at  $K_S = 11.0$  was determined by the fact that at lower magnitudes the locus of the red-clump band becomes difficult to trace due to the small number of sources in this part of the CM diagram. It can be seen from Figure 1 that this selection region is only an approximation to the expected track followed by red-clump stars under a model of uniform extinction per unit distance, but is a reasonable method of selecting such stars in the interval  $11.0 < K_S < 13.5$  (in fact, the faint cut-off adopted in this work is brighter than  $K_S = 13.5$ , see below).

The CM diagram and selection region shown in Figure 1 allows an estimate to be made of the maximum amount of contamination of the red-clump region by main-sequence stars. The profile of the distribution at constant  $K_S$  was examined at  $K_S \approx 13$ . The profile reveals a bimodal distribution with peaks due to main-sequence and evolved stars. At the minimum between the peaks of this distribution, the

density of main-sequence sources is about 10 per cent of the source density in the red-clump band. Since this minimum lies somewhat to the left of the red-clump band, and assuming that the density of main-sequence stars decreases as  $(J - K_S)$  increases, the contamination of main-sequence stars in the selected region will be less than 10 per cent: a reasonable estimate on an upper limit to the contamination would be at the level of a few percent.

In addition to adopting selection criteria which isolate red-clump stars, it is also important to choose a faint cut-off in the value of  $K_S$ . This serves to reduce the bias inherent to detecting excesses at 8  $\mu\text{m}$  when many stars are close to the detection threshold at this wavelength. Ideally, it would be best to select a cut-off in  $K_S$  which results in all sources being detected at 8  $\mu\text{m}$ . However, such a constraint leads to the rejection of a large proportion of the data. I investigated (using Version 1 of GLIMPSE) how the detectability of red-clump sources at 8  $\mu\text{m}$  varies with  $K_S$  and found that at  $K_S = 12.9$ , 85 per cent of sources were detected. This cut-off in  $K_S$  was adopted as being a reasonable compromise between expected detection and source numbers. With these criteria applied ( $11 \leq K_S \leq 12.9$  and Equation 1) the number of red-clump sources selected is 9865. This sample forms the basis of the study of mid-IR excesses.

## 2.2 The selection of sources with 8 $\mu\text{m}$ excess

An indication of the incidence of sources with excesses at 8  $\mu\text{m}$  in the sample is revealed by the  $(K_S - [8.0])$ -( $J - K_S$ ) colour-colour diagram of the selected sample of red-clump sources (Figure 2a). It can be seen that there is a small number (about 20) of sources with excesses in  $(K_S - [8.0])$  which set them clearly apart from the main distribution of sources. Sources with less pronounced, but still significant excesses, can only be identified from more detailed analysis as described below.

It can also be seen from Figure 2a that the effects of interstellar reddening are apparent in the distribution of sources, with a trend for  $(K_S - [8.0])$  to increase with increasing  $(J - K_S)$ . It is therefore useful to define a colour  $(K_S - [8.0])_0$  which includes the effects of reddening. The results of Indebetouw et al. (2005), and in particular, their best-fitting straight line to  $([8.0] - K_S)$ -( $J - K_S$ ) data (as shown in their figure 4a and reproduced here on Figure 2a), allows this to be calculated as

$$(K_S - [8.0])_0 = (K_S - [8.0]) - 0.37 \times (J - K_S) + 0.17 \quad (2)$$

For the sample of red-clump sources described above, the mean value,  $\langle (K_S - [8.0])_0 \rangle$  is  $0.048 \pm 0.002$ . The colour excess of any source is given by a colour excess defined by  $E_{K8} = (K_S - [8.0])_0 - \langle (K_S - [8.0])_0 \rangle$

Sources which are candidates for stars having excesses at 8  $\mu\text{m}$  were selected using the criterion

$$\text{SNR}_{E_{K8}} = \frac{E_{K8}}{\sigma_{E_{K8}}} > 3.7 \quad (3)$$

The significance level here is determined by the sample size: it is chosen such that given a Gaussian distribution in  $E_{K8}$ , it would be expected that there would be only one source in a sample size of  $1 \times 10^4$  which would exceed this value. On applying the above criterion, 52 sources were identified as candidate mid-IR excess sources.

## 3 ANALYSIS OF CANDIDATE 8 $\mu\text{m}$ EXCESS SOURCES

In order to confirm or reject the candidate excess sources, the following approach was taken. Firstly, where doubts exist over the reliability of a source, it was culled from the sample. The remaining sources were then analysed in two ways: on the basis of their near-infrared colours and by modelling of the photometric data.

### 3.1 Removal of low reliability sources

The first stage in checking source reliability was to inspect the GLIMPSE Catalog source quality flag (SQF) for each source. Of the 52 candidate sources, 14 had SQF flags set which indicated confusion in in-band or cross-band merging. Two further sources were flagged as being potentially affected by banding correction and a single source was flagged as being possibly contaminated by stray light.

In addition to the SQF data provided in the GLIMPSE Catalog, the 8  $\mu\text{m}$  GLIMPSE Image Atlas (Version 2) was visually inspected to check for artefacts which might have given rise to anomalous 8  $\mu\text{m}$  fluxes. The highest resolution (0.6 arcsec pixel size) 8  $\mu\text{m}$  GLIMPSE atlas images were used to check for anomalies. Fields of extent 1.2 arcmin around source positions were inspected and six sources (which would have been accepted on the basis of their SQF value of zero) were rejected on the basis of their appearance. Four of these sources appear to be affected by stray light contamination at 8  $\mu\text{m}$ , while two are very close to relatively bright multiple sources. All six of these sources are also deemed to be of questionable reliability and, together with the 17 sources identified by their SQF values, were rejected from the candidate list. The 2MASS and GLIMPSE photometry for the remaining 29 candidate sources is given in Table 1. Note that hereafter, individual sources are referred to by the identifier (ID.) given in this table.

### 3.2 Near-IR colours

Some evidence as to the nature of the stars exhibiting 8  $\mu\text{m}$  excesses can be determined by inspection of the  $(J - H)$ -( $H - K_S$ ) colour-colour diagram (Figure 2b). The locations of the candidate 8  $\mu\text{m}$  excess sources are indicated by the numerical identifier given in Table 1. The vast majority of the sources in this diagram are distributed in a band which corresponds well to the expected location of G/K giants under different amounts of extinction (for reference, a reddening vector is shown which indicates the expected direction of the distribution of stars of type K0III). While the majority of candidate 8  $\mu\text{m}$  excess sources lie within the region populated by reddened G/K giants, it is notable that seven of the candidate excess sources have  $(J - H)$  values which are substantially lower than would be expected from their  $(H - K_S)$  colour (these are sources with identifiers 10, 13, 17, 18, 23, 26 and 29). If these sources are G/K giants, they would appear to have anomalous near-IR colours. The remaining 22 candidate sources appear to be consistent with being G/K giants. Further investigation (below) uses the available 7-band photometry available to model these sources.

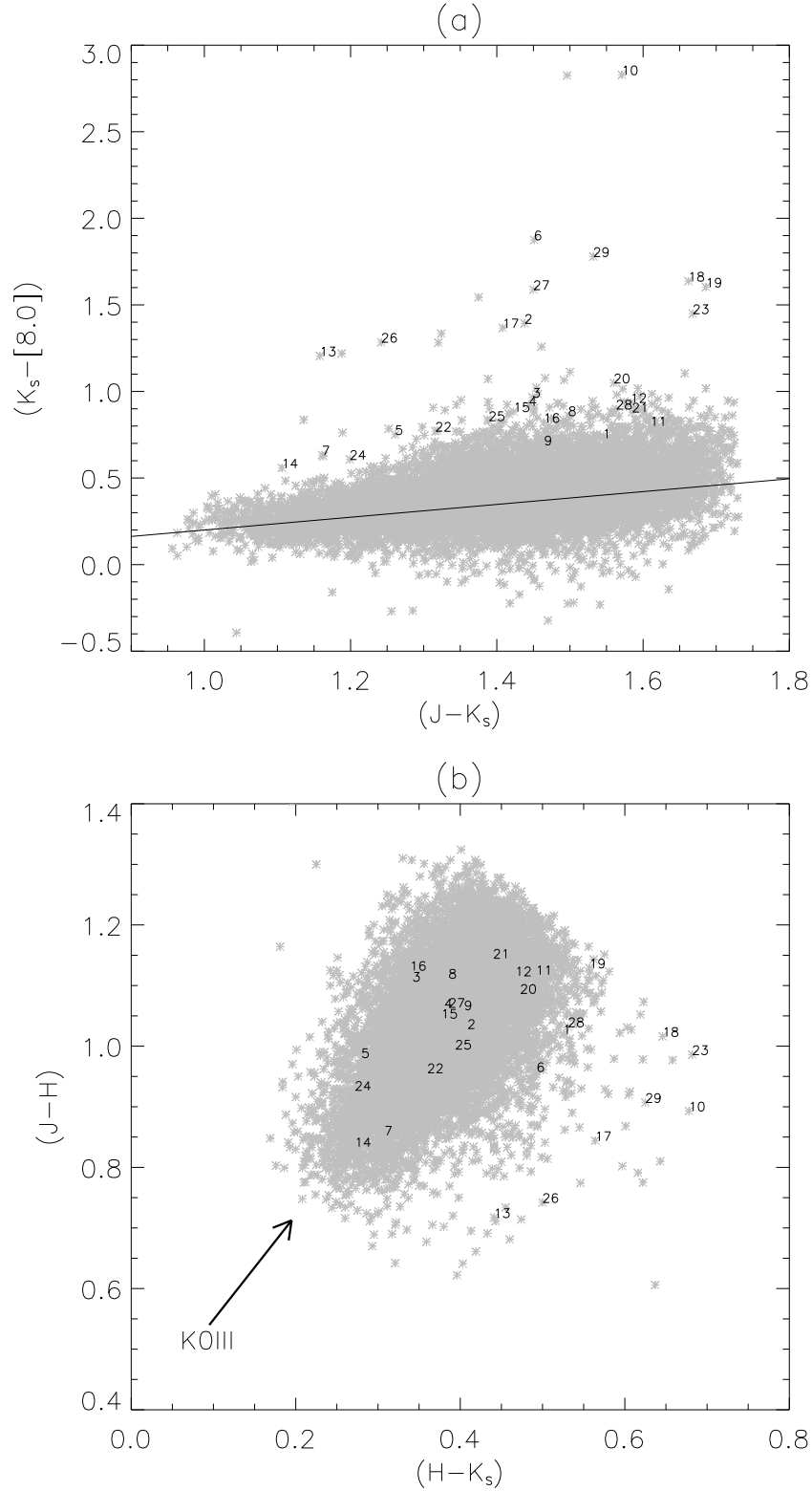


**Figure 2.** Colour-colour diagrams (a)  $(K_S - [8.0])$ - $(J - K_S)$ , and (b)  $(J - H)$ - $(H - K_S)$ , for all of the selected red-clump stars (grey asterisks). Candidate sources with excesses at  $8\ \mu\text{m}$  are indicated by the numerical identifier as given in Table 1. The straight line in (a) shows the extinction relation as derived by Indebetouw et al. (2005) using a similar sample of stars. The reddening vector shown in (b) starts at the expected position of an un-reddened star of type K0III.

Landscape table to go here.

**Table 1.**

### 3.3 Modelling of 7-band photometry

The 29 sources with excesses in their  $(K_S - [8.0])_0$  colours were further analysed to attempt to determine if these sources were likely to be G/K giants with excesses at 8  $\mu\text{m}$ , or if they have some other origin. As noted above, the sample of red-clump stars is expected to be contaminated by other types of source at the level of maybe as much as a few percent. However, it could plausibly be the case that it is these contaminating stars which give rise to the sources detected with 8  $\mu\text{m}$  excesses. Hence it is important then to consider whether the detected excess sources could be other types of star. The approach taken was to use the data from the seven photometric bands ( $J$ ,  $H$ ,  $K_S$ , 3.6  $\mu\text{m}$ , 4.5  $\mu\text{m}$ , 5.8  $\mu\text{m}$ , and 8.0  $\mu\text{m}$ ) to compare to the spectra from a selection of plausible models.

Clearly, one model which needs to be tested is that of a red-clump giant with a mid-IR excess. As a reference point, it is useful to define a ‘canonical’ red-clump giant using the results of the study of Zhao et al. (2001). The subset of metal rich ( $[\text{Fe}/\text{H}] > -0.3$ ) clump giants in their study have a mean effective temperature of  $T_{\text{eff}} = 4860$  K and surface gravity of  $\log g = 2.81$ . The canonical red-clump giant can be approximated by the closest Kurucz model (see below), which has  $T_{\text{eff}} = 4750$  K, and  $\log g = 3.0$ .

In model fitting however, I adopted a range of giant star models with a range of surface temperatures from 3500 K to 6500 K. This is a wider temperature range than would be expected for red-clump giants, but provides a useful check that individual stars are not better modelled as cooler or hotter stars. This, and all other photospheric emission (in other models described below) was modelled using a Kurucz spectral model<sup>2</sup> (Castelli & Kurucz 2004) with solar metallicity (also, the particular set of models used have a turbulent velocity of 2 km s<sup>-1</sup>). The temperature resolution of the published grid of Kurucz models is 250 K.

The mid-IR excess is modelled as a component which only contributes significantly to the 8  $\mu\text{m}$  band. This was implemented as a Gaussian component at a wavelength of 7.9  $\mu\text{m}$  with  $\sigma = 0.6$   $\mu\text{m}$ , with only the normalisation of this parameter being allowed to vary. While this component is a reasonable representation of a PAH feature observed in the spectrum of HD 233517 (Jura et al. 2006) it should be stressed that an excess in one photometric band could be modelled in a variety of ways, and that I do not claim any particular significance to modelling the excess in this way.

A quite different set of stars which are known to show mid-IR excesses are hot stars with infrared excesses arising from bremsstrahlung emission from plasma surrounding the star (Gehrz, Hackwell & Jones 1974). Such sources are detected in considerable numbers by Clarke et al. (2005) and Uzpen et al. (2007) and are believed to occur for stars of spectral type B8 or earlier. Consequently I also examine a hot star model comprising a main-sequence B8 star and bremsstrahlung emission from a plasma at a temperature of  $1 \times 10^4$  K. Note that as far as fitting to the combined 2MASS and GLIMPSE photometry is concerned, the model is rather insensitive to the exact stellar type: the choice of B8V is a conservative one which represents the coolest and lowest lu-

minosity star that might plausibly also exhibit an infrared excess due to bremsstrahlung emission.

A component of all of the fitted models was the inclusion of extinction due to interstellar dust. The extinction values used were taken from the publicly available synthetic extinction curves<sup>3</sup> which are based on the grain model of Li & Draine (2001) and the grain size distribution of Weingartner & Draine (2001). The particular extinction curve used was the one for which  $R_V = 3.1$  and which these authors consider to provide a good match to the extinction properties of diffuse HI clouds in the Milky Way.

For all of the models, three parameters were fitted: the normalisation  $X$  of the stellar spectral component, the normalisation of either the bremsstrahlung component or of the Gaussian line at 7.9  $\mu\text{m}$ , and the line-of-sight column density  $N_H$ . In addition to these parameters, note that for the red-clump giant model, the fitting was conducted across a range of temperatures (as described above) in order to also determine the photospheric temperature. A spectrophotometric distance  $d$  to the star can be derived from the normalisation parameter  $X$  by  $d = r_* X^{-1/2}$  where  $r_*$  is the stellar radius. Stellar radii were estimated by assuming blackbody emission and relationships between stellar luminosity and temperature as given by de Jager & Nieuwenhuijzen (1987).

It is important to appreciate that the spectral resolution provided by the seven photometric bands used here is, in general, insufficient to provide any clear discrimination in luminosity class: data which are well modelled as a G/K giant with a Gaussian excess at 8  $\mu\text{m}$ , will also be acceptably fitted by models in which the star is a G/K dwarf or supergiant. Models in which the star is modelled as a dwarf and as a supergiant were also fitted to obtain spectrophotometric distances and values of column density for the excess sources. In order to investigate whether these models could be plausible, a set of neighbouring (non-excess) red-clump giants was used to estimate the column density in the direction of each candidate excess source. The set of neighbouring sources for each candidate excess source was defined as those sources which were selected according to the red-clump criterion (Equation 1) and which lie within 5 arcmin of the position of the excess source and which have  $K_S$  within 0.2 mag of this source. In fitting to these neighbouring red-clump giants, the canonical red-clump stellar model was assumed (i.e.  $T_{\text{eff}} = 4750$  K, and  $\log g = 3.0$ ). The fitting process returned a column density and flux normalisation ( $X$ ) for each source, allowing a mean column density and mean spectrophotometric distance for the neighbouring red-clump stars to be determined. These values for a so-called ‘neighbouring field’ are given in Table 2 and are discussed further in Section 3.4.

For a particular model, the expected flux density in each photometric band was obtained by integrating uniformly over a passband between the wavelengths at which the filter response is half its maximum value. Such an integration is an approximation to modelling the exact photometric responses of the filters, but is expected to be adequate for this work.

The fitting process was a minimisation of chi-squared type approach, using the MPCURVEFIT routine in IDL.

<sup>2</sup> Obtained from <http://wwwuser.oat.ts.astro.it/castelli/grids.html>

<sup>3</sup> <http://www.astro.princeton.edu/~draine/dust/dustmix.html>

ID.	Designation	Type	$T/K$	$\chi^2_\nu$	Best fit model		$E_8$	SNR <sub>8</sub>	Neighbouring field	
					$N_H$	$d/kpc$			$N_H$	$d/kpc$
1	G045.1000+00.8808	RCG	5750	0.69	$12.7 \pm 0.5$	$2.1 \pm 0.4$	0.13	2.3	$8.3 \pm 1.0$	4.4
2	G045.1844+00.7612	RCG	5000	0.33	$9.8 \pm 0.9$	$4.4 \pm 1.0$	0.89	9.2	$9.1 \pm 1.1$	5.4
3	G045.2769+00.7123	RCG	4500	0.40	$7.9 \pm 0.9$	$6.7 \pm 1.7$	0.52	3.9	$9.1 \pm 1.1$	5.4
4	G045.2852+00.9988	RCG	4500	0.41	$7.7 \pm 1.0$	$7.0 \pm 2.1$	0.52	5.0	$9.2 \pm 0.8$	5.5
5	G045.4108+00.8768	RCG	4500	0.38	$5.8 \pm 0.9$	$5.9 \pm 1.5$	0.42	5.7	$7.4 \pm 2.4$	4.6
7	G046.2397+00.9526	RCG	5000	0.13	$6.6 \pm 0.6$	$2.7 \pm 0.4$	0.28	5.9	$6.8 \pm 1.3$	3.3
8	G046.3252+00.8710	RCG	4750	0.58	$9.6 \pm 0.7$	$5.4 \pm 1.1$	0.33	4.2	$9.2 \pm 1.1$	5.5
9	G046.6118+00.9688	RCG	4500	0.81	$8.0 \pm 0.9$	$5.2 \pm 1.3$	0.27	4.0	$8.3 \pm 0.9$	4.1
10	G046.6781+00.7324	HSB	11500	0.66	15.2	$> 1.8$	2.45	82		
11	G046.6833+00.8797	RCG	4500	0.90	$9.3 \pm 0.9$	$6.1 \pm 1.5$	0.35	4.6	$9.6 \pm 0.9$	4.9
12	G046.7233+00.7512	RCG	4250	1.05	$7.9 \pm 0.8$	$8.6 \pm 2.2$	0.54	4.5	$9.8 \pm 0.7$	5.2
13	G046.9192+00.7417	HSB	11500	0.65	13.1	$> 1.1$	0.65	19		
14	G047.5359+00.8104	RCG	5750	1.96	$8.3 \pm 0.6$	$1.8 \pm 0.3$	0.12	2.7	$7.6 \pm 1.0$	3.3
15	G047.8477+00.9287	RCG	4000	1.36	$4.9 \pm 0.6$	$8.6 \pm 3.2$	0.64	5.4	$7.6 \pm 1.0$	4.0
16	G048.1801+00.9573	RCG	4250	0.26	$6.9 \pm 1.1$	$8.2 \pm 2.2$	0.43	4.3	$8.4 \pm 0.9$	5.1
17	G048.3706+00.7076	HSB	11500	1.24	15.3	$> 1.7$	0.75	11		
19	G048.3924+00.8103	RCG	5000	0.78	$12.1 \pm 1.1$	$4.4 \pm 1.5$	1.04	12	$9.5 \pm 1.3$	5.5
20	G048.4911+00.8260	RCG	4500	0.96	$9.2 \pm 1.1$	$6.2 \pm 1.9$	0.57	4.0	$9.0 \pm 1.1$	5.1
21	G048.5964+00.7855	RCG	4500	0.15	$9.2 \pm 0.8$	$6.5 \pm 1.6$	0.40	3.9	$9.7 \pm 1.1$	5.2
22	G048.5970+00.9849	RCG	4750	0.74	$7.2 \pm 0.8$	$5.5 \pm 1.2$	0.40	4.0	$8.4 \pm 1.1$	5.2
23	G048.6036+00.9284	HSB	11500	0.51	17.7	$> 1.6$	0.75	12		
24	G049.0793+00.7610	RCG	4500	0.57	$5.0 \pm 1.0$	$5.6 \pm 1.6$	0.33	4.6	$7.4 \pm 1.2$	4.3
25	G049.1099+00.8232	RCG	4500	0.59	$7.0 \pm 0.9$	$6.5 \pm 1.6$	0.48	5.2	$8.7 \pm 1.1$	5.1
26	G049.4210+00.8476	HSB	11500	0.60	13.5	$> 1.6$	0.76	11		
27	G049.5812+00.9666	RCG	4250	0.30	$6.8 \pm 1.0$	$8.6 \pm 2.9$	1.23	7.2	$8.0 \pm 0.9$	5.4
28	G049.9290+00.8456	RCG	6250	0.32	$14.0 \pm 0.6$	$1.8 \pm 0.3$	0.23	3.0	$9.2 \pm 1.0$	5.6
29	G050.1256+00.9808	HSB	11500	0.57	16.3	$> 1.6$	1.15	26		

**Table 2.** The results of model fitting. Column 1 shows the source identifier (ID.) as used in Table 1. Column densities ( $N_H$ ) are expressed in units of ( $10^{21}$  H atoms  $\text{cm}^{-2}$ ). The quantities  $E_8$  and SNR<sub>8</sub> are defined in the text.

Given that fitting was carried out at fixed photospheric temperatures, the uncertainties in the fitted parameters which were returned by this process were unrealistically small. Consequently, uncertainties in fitted parameters (and quantities derived from these parameters) were estimated by inspection of the parameters returned from a range of temperatures corresponding to variation in  $\chi^2$  of about 1.

### 3.4 Results of modelling

The modelling process has two distinct aims. The first is to determine whether a given excess source can be acceptably fitted by a model which comprises a red-clump giant and Gaussian excess at  $8 \mu\text{m}$  (a model referred to here as RCG) or by a model comprising a hot star and bremsstrahlung emission (which is referred to as HSB). The second aim is to determine which of the those stars which are well modelled by the RCG model do actually exhibit a significant excess at  $8 \mu\text{m}$ .

Of the 29 candidate sources, 27 could be fitted by either the RCG or HSB models within the 95 per cent confidence interval and are taken to be acceptably modelled. The two sources (6 and 18) which were not acceptably fitted had minimum values of  $\chi^2_\nu > 5$  and hence the models can be rejected at the 99.9 percent confidence level. The spectral energy distribution of source 6 (shown in Figure 3, left-hand panel) suggests that it has a continuum level which differs between the 2MASS and GLIMPSE observations. Since 2MASS and GLIMPSE data were collected at different times, a likely explanation is that this is a variable star and it is discounted

from any further analysis. The nature of source 18 is less clear: this could be an RCG source with infrared excesses at as short a wavelength as  $4.5 \mu\text{m}$ , although its spectral energy distribution (Figure 3, right-hand panel) also appears to be reasonably well-described by the HSB model with the exception of the flux measurement at  $3.6 \mu\text{m}$ . While it is possible that variants to the RCG or HSB model could describe the data for this source, such modelling is not justified using these data. It is also noted that this source is one of the seven sources in Figure 2b which lie away from the expected distribution of G/K giants (see Section 3.2). The nature of source 18 is acknowledged to be uncertain and this source is excluded from further analysis.

For all of the sources which can be acceptably fitted by either the RCG or the HSB models, an excess at  $8 \mu\text{m}$  (called  $E_8$ ) was determined by calculating the difference between the observed value of  $[8.0]$  and the model photospheric value ( $[8.0]_{\text{phot}}$ ). The signal-to-noise ratio of the excess was calculated as

$$\text{SNR}_8 = \frac{[8.0] - [8.0]_{\text{phot}}}{\sigma_{[8.0]}} \quad (4)$$

This quantity is tabulated, along with the results of the model fitting in Table 2.

Of the 27 sources which are well modelled by either the HSB or RCG models, it should be noted that the distinction between these two classes of models is very strong: no source can be acceptably modelled by both types of model. Six of the 27 sources are better fitted by the HSB model than by the RCG model, and all of these sources were identified from Figure 2 as being unlikely to be G/K



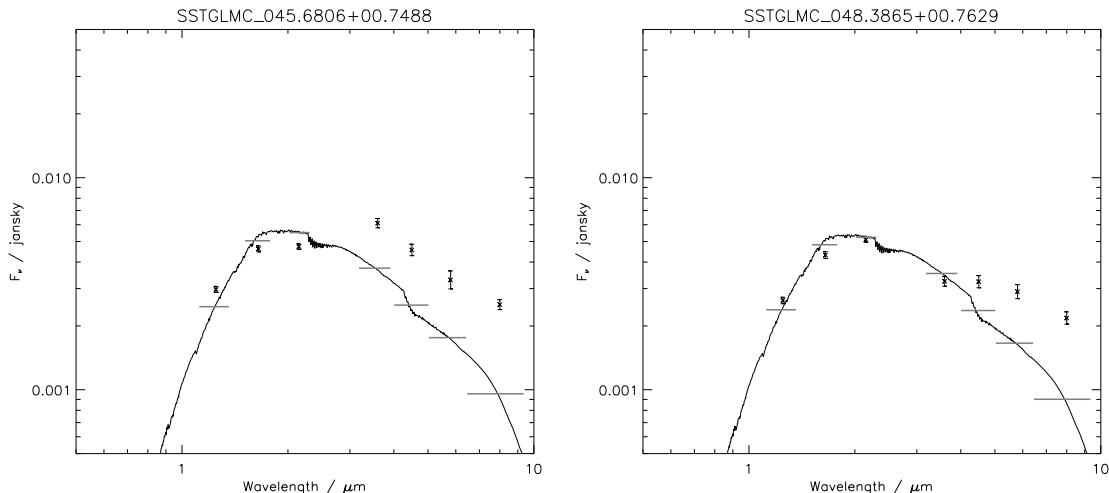


**Figure 3.** The spectral energy distributions of the two candidate excess sources (6 and 18, shown on left and right respectively) which are not well fitted by either the RCG or HSB models (see text). Photometric data points are indicated by 'x' with error bars. For comparison the spectrum of a canonical red-clump giant is also shown (continuous line) together with the model photometric points (grey bars - the width of which represent the FWHM of the photometric bands).

giants. The sources are characterised by high column densities ( $> 10^{22}$  H atoms  $\text{cm}^{-2}$ ) and very strong mid-IR excesses ( $\text{SNR}_8 > 10$ ). Note that because the model assumes the star is the lowest luminosity star which is likely to exhibit bremsstrahlung emission (i.e. type B8V) the distances quoted in Table 2 are lower limits. Two examples of the spectral energy distribution of sources that are best fitted by the HSB model are shown in Figure 4. It is noticeable that this model can reproduce a wide range of spectral slopes at  $\lambda > 2 \mu\text{m}$ . In particular, the source 10 seems to have spectral energy distribution which rises between the 2MASS and the GLIMPSE bands, and it is clear that this behaviour can be successfully described by the HSB model.

The remaining 21 sources are well-fitted by the RCG model, and it is notable that in Figure 2, all of these sources are at locations consistent with them being G/K giants. The quantity  $\text{SNR}_8$  is used to determine whether the excess at  $8 \mu\text{m}$  is confirmed. As in the case for selecting candidate excess sources using  $E_{K8}$ , the cut-off is at a level where only one excess source is expected to occur by chance from the total sample of red-clump giants, i.e.  $\text{SNR}_8 > 3.7$ . Of the 21 candidate excess sources which can be fitted by the RCG model, 18 show excesses which satisfy this criterion, and of these, seven sources have  $\text{SNR}_8 \geq 5$ .

Three sources (1, 14, and 28) do not have confirmed excesses. It is noticeable that these are all of high photospheric temperature ( $T_{\text{eff}} = 5750$  K, 6250 K). Such temperatures would be unusually high for a red-clump star, and it is possible that these stars are low metallicity stars on the horizontal branch. However, given that their mid-IR excesses are unconfirmed, they are rejected from the sample.

The remaining 18 sources are strong candidates for being G/K giants with mid-IR excess. Examples of the spectral energy distributions of two of these sources are shown in Figure 5. As might be expected from the goodness-of-fit for these sources, the RCG model provides an excellent match to these data, with no indication of systematic deviations which might cause us to question the validity of the model. However, one possibility that should be addressed is

that these stars might be of a different luminosity class to that assumed in the model, i.e. that the stars may be on the main-sequence or supergiants.

This was investigated by fitting using Kurucz models corresponding to G/K dwarfs and supergiants (using Version 1 of the GLIMPSE data). In the case of models which are well-fitted as red-clump giants, the best-fitting dwarf or supergiant model typically has a very similar temperature (usually differing by no more than 250 K) and similar column density to the best-fitting giant star model. The distance estimates, as would be expected, depend very strongly on the assumed luminosity class. As can be seen from Table 2 the distances implied by giant star models are broadly consistent with those obtained from the neighbouring red-clump stars (labelled as the 'neighbouring field' in Table 2). Dwarf star models (luminosity class V) imply distances which are typically an order of magnitude lower than the mean distance to the neighbouring red-clump giants, but at a similar value of total column density. It is concluded that it is highly unlikely that any of the candidate excess stars are on the main-sequence. The distance estimates which are arrived at assuming that the candidate excess star is a supergiant of luminosity class I are typically of order 100 kpc. The assumption that these stars are supergiants can be rejected since such distances would place these stars well outside the stellar disc of the Milky Way. It seems reasonable to conclude that the candidate excess stars are all giants (i.e. luminosity class III).

## 4 DISCUSSION

The analysis presented here confirms that there is a population of red-clump stars which appear to be G/K giants with significant mid-IR excesses. Out of an initial sample of 9865 red-clump stars, the analysis presented here identifies 18 sources which fall into this category. The incidence of mid-IR excesses in G/K giants is thus calculated to be  $(1.8 \pm 0.4) \times 10^{-3}$ . This is substantially lower than the in-

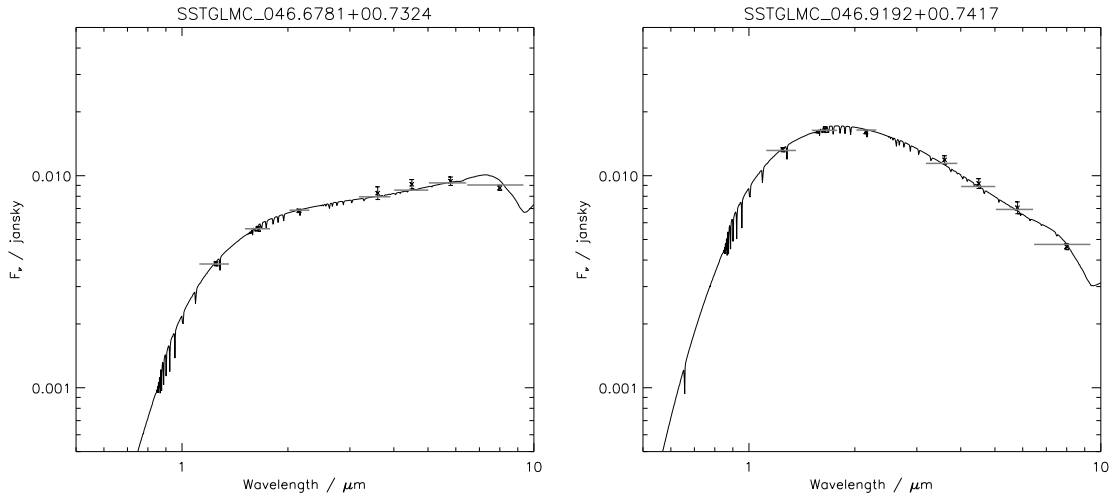


**Figure 4.** The spectral energy distributions of two excess sources (10 and 13, shown on left and right respectively) which are well fitted by HSB models (see text). These two examples illustrate the wide range of continuum slope which can be generated by this model. The spectral energy distributions are displayed in the same manner as in Figure 3.

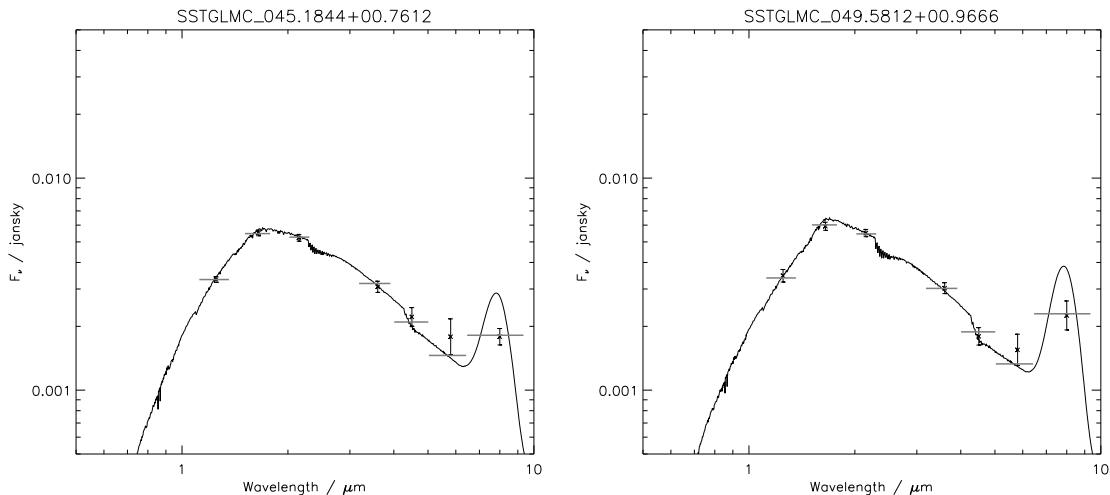


**Figure 5.** The spectral energy distributions of two excess sources (2 and 27, shown on left and right respectively) which are well fitted by RCG models (see text). These are the two sources of this type with the strongest 8  $\mu\text{m}$  excesses. The spectral energy distributions are displayed in the same manner as in Figure 3.

cidence of far-IR excesses in G/K giants of  $14 \pm 5$  percent reported by Plets & Vynckier (1999). This low-incidence of mid-IR excesses as compared to far-IR excesses mirrors, in a qualitative sense at least, the behaviour seen for main-sequence stars, where mid-IR excesses are far less common than those detected at far-IR wavelengths, which is interpreted as reflecting the incidence of systems with hot ( $\sim \text{few} \times 100$  K) and cold ( $< 100$  K) dust respectively (Uzpen et al. 2007). A discussion of implications of our observed incidence of mid-IR excesses in G/K giants is given below.

In investigating candidate excess sources, this work has also identified a substantial number of sources whose SEDs are well-described as highly absorbed early-type stars in which the excess emission arises from bremsstrahlung emission (the HSB model). With the admittedly limited information provided by the 7-band photometry used here, some caution should be expressed about the physical interpreta-

tion of this model: it may plausibly be the case that this type of SED is produced by a G/K giant (or other luminous star) which has infrared excesses across most of the photometric bands used here. An argument against this view is however provided by the  $(J - H)$ - $(H - K_s)$  diagram (Figure 2). When the suspected variable star (source 6) and the high-temperature RCG sources (1, 28 and 14) are removed from the diagram, the distinction between RCG and HSB models becomes quite clear, with the HSB stars seeming to follow an extinction vector which is distinct from that followed by G/K giants. If the stars which are here classified as HSB were simply RCG stars with different types of infrared excess, then such a distinct separation would not be expected. So it seems likely that the stars modelled as HSB type are distinct from G/K giants, although without spectroscopic identification of the stellar types, it cannot be confirmed that the hot-star plus bremsstrahlung model provides the correct physical interpretation for these sources.

It is also of interest to examine whether the number of HSB sources detected here is consistent with the known frequency of early-type stars with bremsstrahlung emission. This work reveals six such sources in a survey area of  $1.575 \text{ deg}^2$ , i.e., at a surface density of about  $4 \text{ deg}^{-2}$ . Sources of this type are ubiquitous in studies of mid-IR excess: Uzpen et al. (2007) report 126 such sources, which corresponds to a surface density (in the GLIMPSE survey region) of about  $0.6 \text{ deg}^{-2}$ . In that work however, the typical  $K_S$  magnitude of the early-type star involved is about 8. The work presented here is sensitive to  $K_S \leq 12.9$ . A crude extrapolation (based on a uniform spatial distribution of sources) of the surface density of these sources from the work of Uzpen et al. (2007) to the flux limits adopted here yields a value of order  $100 \text{ sources deg}^{-2}$ . It does not seem unreasonable then that a small fraction of such sources fall within the region of the  $K_S/(J - K_S)$  colour magnitude diagram used to isolate RCG stars.

Turning now to the sources which are identified as being G/K giants with excesses at  $8 \mu\text{m}$ , a key question relates to the nature of the observed mid-IR excess. If the emission arises from a debris disc, it might be expected that the spectrum of the emission would be reasonably well approximated by a blackbody spectrum. Given that the photometric data presented here do not extend to wavelengths beyond  $8 \mu\text{m}$ , it is not possible to determine a blackbody temperature of the component giving rise to the mid-IR excess. However, an estimate can be made on the upper limit to the blackbody temperature, by requiring that the excess component does not exceed measured values at  $5.8 \mu\text{m}$ . Inspection of blackbody models in comparison to the SEDs of two strong excess sources (2 and 27, whose SEDs are shown in Figure 5) reveals that models in which mid-IR emission arises from a blackbody component are a good representation of the data when the blackbody temperatures are lower than about 450 K, and temperatures in excess of 600 K can clearly be ruled out.

Another possible source of mid-IR emission is from PAHs. This is particularly pertinent to this study as one of the few G/K giants which has been subject to mid-IR spectroscopy, HD 233517 (Jura et al. 2006), shows strong PAH emission. In the  $8 \mu\text{m}$  band, the infrared excess of this K2III star is dominated by PAH emission which has an amplitude which is approximately 70 percent of the photospheric emission in this band (estimated from figure 1 of Jura et al.). The model used here to describe red-clump giants with mid-IR excesses included a Gaussian component which was chosen to provide a reasonably good representation of the  $7.9 \mu\text{m}$  PAH feature in the spectrum of HD 233517. I note that several sources have  $8 \mu\text{m}$  excesses of about 0.5 magnitudes, which corresponds to the relative amplitude of Gaussian component with respect to the photospheric emission being similar to that observed in HD 233517. On the basis of these data I would not claim that PAH emission is the dominant cause of mid-IR excesses all G/K giants, but note that it is a possibility which deserves further investigation.

It is also of interest to examine the consequences of the measured incidence of mid-IR excesses in G/K giants in relation to the corresponding incidence in their main-sequence precursors. It is known that main-sequence stars give rise to mid-IR excesses which most likely arise from hot dust in debris discs. Dust is produced by collisions within debris discs

but its emission depends on the radiation field of the host star. As a star with a disc evolves beyond the main-sequence, it is likely that the collisional processes are relatively unaffected, whereas the radiation environment changes as the luminosity (and temperature) of the star change. An increase in luminosity of the host star between the main-sequence and the red-clump has two distinct effects. The first is that the blackbody temperature of dust (at a given radius from the star) will increase by a factor  $(L_{\text{RC}}/L_{\text{MS}})^{1/4}$ , where  $L_{\text{MS}}$  and  $L_{\text{RC}}$  are the stellar luminosities on the main-sequence and in the red-clump respectively. Secondly, if the lifetime ( $t_{\text{pr}}$ ) of dust (i.e. from its generation to its accretion onto, or sublimation close to, the star) is determined by Poynting-Robertson (P-R) drag, then this lifetime will vary according to

$$\frac{t_{\text{pr,RC}}}{t_{\text{pr,MS}}} = \frac{L_{\text{MS}}}{L_{\text{RC}}} \quad (5)$$

(where the subscripts MS and RC refer to main-sequence and red-clump respectively). While the assumption of the importance of P-R drag would be contrary to the theoretical expectation that dust lifetimes are determined by collisional timescales in massive debris discs (Wyatt 2005), it is useful to explore such a scenario in the light of the results presented in this paper.

In order to analyse how these changes might have an impact on the observations presented here, it is necessary to identify the main-sequence precursors to red-clump stars. While recognising that red-clump stars, can in principle, have a relatively wide range of masses ( $0.5M_{\odot}$  to  $2.5M_{\odot}$ , see e.g. Zhao et al. 2001) I choose a value of  $2M_{\odot}$  as being representative of the mass of the main-sequence precursor. This would correspond to spectral type A5V, with a luminosity of about  $12L_{\odot}$ . If such a star evolves to form a canonical red-clump star, its luminosity would increase to about  $46L_{\odot}$ .

The effect that this would have on dust temperature is that it would increase by about 40 per cent. The detection of a difference in mean temperatures between a population of main-sequence stars and red-clump stars would require a much more comprehensive survey of mid-IR spectra than are currently available and certainly would require longer wavelength data than used in this study. Even if such a survey could be conducted, the known variation in main-sequence disc temperatures, ranging from about 200 K to 800 K (Uzpen et al., 2007) would make it very difficult to interpret such a study.

On the other hand, the effect of variation of stellar luminosity on  $t_{\text{pr}}$  may have more readily apparent observable consequences. Under the assumption that dust lifetimes are dominated by P-R drag, then provided that dust is generated by episodic events (such as in the solar system, e.g. Farley et al. 2006), and that the mean interval between dust generating events is much greater than  $t_{\text{pr}}$ , then the incidence of mid-IR excesses will be proportional to  $t_{\text{pr}}$ .

The observed incidence of mid-IR excesses in A type main-sequence stars is reported by Uzpen et al. (2007) as  $1.0 \pm 0.5$  per cent. Using the values given above for  $L_{\text{MS}}$  and  $L_{\text{RC}}$ , the ratio of the decay timescales  $t_{\text{pr,RC}}/t_{\text{pr,MS}} = 0.27$ , and within the scenario described above, this should correspond to the ratio of incidences of mid-IR excesses. Hence the expected incidence of mid-IR excesses in G/K

giants would be expected to be  $(2.7 \pm 1.4) \times 10^{-3}$ . This is in agreement with our observed value of  $(1.8 \pm 0.4) \times 10^{-3}$ . Hence, a model in which dust lifetimes in debris discs are dominated by P-R drag leads to a natural explanation of the observed incidence of mid-IR excesses in G/K giants.

## 5 CONCLUSIONS

The major conclusion of this study is that mid-IR excesses are exhibited by G/K giants albeit at a very low level of incidence. This could be consistent with the level of mid-IR excesses in their main-sequence precursors provided that dust generation is episodic and dust lifetimes are determined by P-R drag rather than collisional processes. In passing, I note that this work has obtained a value for the incidence of mid-IR excesses in G/K giants which is better determined than the corresponding incidence in main-sequence stars. While it is assumed here that the mid-IR emission arises from relatively large dust grains in a debris disc, it should be emphasised that the nature of the mid-IR emission in this population remains uncertain, and requires mid-IR spectroscopic investigation.

This study has illustrated that the technique of isolating samples of red-clump stars from CM diagrams can be a useful technique to study this population of stars. I would expect that this technique could be put to good use by its application to a study of the incidence of excesses at longer infrared wavelengths.

## ACKNOWLEDGMENTS

This publication makes use of data products from the Two Micron All Sky Survey, which is a joint project of the University of Massachusetts and the Infrared Processing and Analysis Center/California Institute of Technology, funded by the National Aeronautics and Space Administration and the National Science Foundation. I should like to thank Glenn White and the anonymous referee for comments which have helped to improve this paper.

## REFERENCES

- Becklin E.E., Farihi J., Jura M., Song I., Weinberger A.J., Zuckerman B., 2005, *ApJ*, 632, L119
- Benjamin R. et al., 2003, *PASP*, 115, 953
- Bessell M.S., Brett J.M., 1988, *PASP*, 100, 1134
- Castelli F., Kurucz R., 2004, preprint (arXiv:astro-ph/0405087)
- Clarke A.J., Oudmaijer R.D., Lumsden S.L., 2005, *MNRAS*, 363, 1111
- Cox A.N., 2000, *Allen's Astrophysical Quantities*, 4th ed. AIP Press; Springer, New York
- de Jager C., Nieuwenhuijzen H., 1987, *A&A*, 177, 217
- Dame T.M., Hartmann D., Thaddeus P. 2001, *ApJ*, 547, 792
- Farley K.A.; Vokrouhlický D., Bottke W.F., Nesvorný D., 2006, *Nature*, 439, 7074
- Fazio G. et al., 2004, *ApJS*, 154, 10
- Gehrz R.D., Hackwell J.A., Jones T.W., 1974, *ApJ*, 191, 675
- Indebetouw R. et al., 2005, *ApJ*, 619, 931,
- Jura M., 1999, *ApJ*, 515, 706
- Jura M. et al., 2006, *ApJ*, 637, L45
- Li A., Draine B.T., 2001, *ApJ*, 554, 778
- López-Corredoira M., Cabrera-Lavers A., Garzón F., Hammersley P. L., 2002, *A&A*, 394, 883
- Marshall D. J., Robin A. C., Reylé C., Schultheis M., Picaud, S., 2006, *A&A*, 453, 635
- Moshir M. et al., 1992, *IRAS Faint Source Survey Explanatory Supplement*. Version 2.0. JPL D-10015 8/92, JPL, Pasadena
- Plets H., Vynckier C., 1999, *A&A*, 343, 496
- Skrutskie M.F. et al., 2006, *AJ*, 131, 1163
- Su K. Y. L. et al., 2007, *ApJ* 657, L41
- Uzpen B. et al., 2007, *ApJ*, 658, 1264
- Weingartner J.C., Draine B.T., 2001, *ApJ*, 548, 296
- Wright C.O., Egan M.P., Kraemer K.E., Price S.D., 2003, *AJ*, 125, 359
- Wyatt M.C., 2005, *A&A*, 433, 1007
- Zuckerman B., Becklin E.E., 1987, *Nature*, 330, 138
- Zhao G., Qiu H.M., Mao S., 2001, *ApJ*, 551, L85

ID.	Designation	$J$	$\sigma(J)$	$H$	$\sigma(H)$	$K_S$	$\sigma(K_S)$	[3.6]	$\sigma([3.6])$	[4.5]	$\sigma([4.5])$	[5.8]	$\sigma([5.8])$	[8.0]	$\sigma([8.0])$	$E_{K8}$	$\text{SNR}_{E_{K8}}$
1	G045.1000+00.8808	13.759	0.034	12.739	0.029	12.214	0.029	11.745	0.049	11.688	0.051	11.451	0.081	11.484	0.057	0.280	4.2
2	G045.1844+00.7612	14.202	0.035	13.173	0.033	12.764	0.040	12.390	0.066	12.272	0.110	12.036	0.211	11.371	0.097	0.983	9.2
3	G045.2769+00.7123	14.212	0.037	13.105	0.029	12.763	0.032	12.397	0.058	12.438	0.090	12.223	0.152	11.797	0.134	0.552	4.0
4	G045.2852+00.9988	14.242	0.060	13.179	0.053	12.798	0.051	12.523	0.066	12.430	0.066	12.518	0.189	11.881	0.104	0.505	4.2
5	G045.4108+00.8768	13.589	0.033	12.608	0.062	12.328	0.033	12.062	0.061	12.135	0.080	11.886	0.117	11.577	0.074	0.406	4.9
6	G045.6806+00.7488	14.323	0.035	13.365	0.035	12.872	0.033	11.644	0.054	11.487	0.067	11.371	0.106	10.997	0.059	1.460	20.9
7	G046.2397+00.9526	12.690	0.021	11.837	0.021	11.529	0.020	11.245	0.052	11.231	0.050	11.233	0.087	10.896	0.047	0.325	6.2
8	G046.3252+00.8710	14.369	0.031	13.257	0.026	12.871	0.033	12.442	0.053	12.399	0.061	12.439	0.128	12.011	0.080	0.428	4.9
9	G046.6118+00.9688	13.640	0.023	12.580	0.022	12.175	0.023	11.842	0.047	11.883	0.067	11.598	0.095	11.484	0.066	0.271	3.8
10	G046.6781+00.7324	14.045	0.024	13.152	0.029	12.474	0.018	11.314	0.075	10.736	0.055	10.231	0.050	9.645	0.030	2.370	64.6
11	G046.6833+00.8797	14.187	0.032	13.069	0.030	12.577	0.028	12.274	0.062	12.291	0.091	12.057	0.114	11.776	0.076	0.327	4.0
12	G046.7233+00.7512	14.333	0.045	13.217	0.043	12.750	0.026	12.524	0.075	12.458	0.055	12.222	0.131	11.814	0.120	0.472	3.8
13	G046.9192+00.7417	12.700	0.024	11.983	0.033	11.542	0.024	10.921	0.048	10.728	0.058	10.544	0.070	10.337	0.035	0.899	20.3
14	G047.5359+00.8104	12.701	0.025	11.867	0.033	11.595	0.025	11.210	0.053	11.097	0.051	11.221	0.067	11.037	0.045	0.271	5.1
15	G047.8477+00.9287	13.454	0.028	12.408	0.033	12.031	0.026	11.864	0.052	11.952	0.083	11.648	0.103	11.148	0.119	0.479	3.9
16	G048.1801+00.9573	14.089	0.022	12.964	0.035	12.625	0.033	12.253	0.076	12.362	0.095	12.140	0.255	11.804	0.100	0.401	3.8
17	G048.3706+00.7076	13.977	0.025	13.133	0.031	12.569	0.023	11.985	0.052	11.702	0.068	11.277	0.076	11.202	0.066	0.968	13.6
18	G048.3865+00.7629	14.454	0.038	13.438	0.040	12.792	0.028	12.330	0.058	11.861	0.072	11.509	0.083	11.155	0.072	1.144	14.4
19	G048.3924+00.8103	14.562	0.033	13.433	0.043	12.876	0.032	12.430	0.053	12.466	0.095	12.093	0.147	11.273	0.089	1.101	11.5
20	G048.4911+00.8260	14.201	0.055	13.114	0.063	12.641	0.054	12.200	0.056	12.423	0.120	12.147	0.131	11.592	0.142	0.594	3.8
21	G048.5964+00.7855	14.337	0.036	13.192	0.037	12.752	0.035	12.368	0.049	12.411	0.076	12.205	0.145	11.871	0.104	0.417	3.7
22	G048.5970+00.9849	14.024	0.035	13.068	0.031	12.708	0.027	12.492	0.065	12.448	0.085	12.199	0.128	11.938	0.101	0.405	3.8
23	G048.6036+00.9284	14.306	0.038	13.320	0.037	12.638	0.048	11.984	0.055	11.746	0.082	11.456	0.087	11.189	0.062	0.954	11.7
24	G049.0793+00.7610	13.365	0.022	12.438	0.030	12.166	0.021	12.000	0.048	11.979	0.069	11.825	0.089	11.559	0.072	0.285	3.8
25	G049.1099+00.8232	13.995	0.032	13.000	0.031	12.606	0.044	12.327	0.058	12.408	0.094	12.128	0.123	11.775	0.092	0.439	4.2
26	G049.4210+00.8476	13.558	0.035	12.816	0.033	12.316	0.050	11.808	0.062	11.450	0.071	11.204	0.091	11.032	0.066	0.946	11.0
27	G049.5812+00.9666	14.158	0.074	13.094	0.048	12.708	0.043	12.406	0.064	12.501	0.103	12.191	0.185	11.120	0.171	1.174	6.6
28	G049.9290+00.8456	13.804	0.050	12.772	0.062	12.241	0.030	11.729	0.055	11.512	0.071	11.546	0.094	11.343	0.076	0.442	5.2
29	G050.1256+00.9808	13.990	0.041	13.083	0.049	12.458	0.037	11.712	0.075	11.417	0.079	11.148	0.070	10.679	0.044	1.334	21.9

**Table 1.** Photometric data for reliable sources selected as candidates for having 8  $\mu\text{m}$  excesses. Column 1 (ID.) is the identifier used to refer to individual sources in this paper. For each photometric band  $\sigma()$  represent the single standard deviation uncertainties. The quantities  $E_{K8}$  and  $\text{SNR}_{E_{K8}}$  are defined in the text.